Water-soluble polythiophenes as efficient charge-transport layers for the improvement of photovoltaic performance in Bulk Heterojunction polymeric solar cells

Massimiliano Lanzi[a]*, Elisabetta Salatelli[a], Loris Giorgini[a], Adele Mucci[b], Filippo Pierini[c], Francesco Paolo Di-Nicola[a]

[a] *Department of Industrial Chemistry "Toso Montanari", University of Bologna, Viale Risorgimento 4, 40136 Bologna (Italy)*

[b] *Department of Chemical and Geological Sciences, University of Modena and Reggio Emilia, Via G. Campi 103, 41125 Modena (Italy)*

[c] *Institute of Fundamental Technological Research, ul. Pawinskiego 5B, 02-106 Warsaw (Poland)*

*Corresponding author. *E-mail address:* massimiliano.lanzi@unibo.it (M. Lanzi).

ABSTRACT

Water-soluble regioregular poly{3-[(6-sodium sulfonate)hexyl]thiophene} (PT6S) and poly{3-[(6-trimethylammoniumbromide)hexyl]thiophene} (PT6N) have been synthesized and employed both as photoactive layers for the assembling of "green" bulk-heterojunction organic solar cells and as charge-collection layers in a cell with "classic" architecture. While the photovoltaic performances obtained with the two aforementioned polymers were lower than the reference cell, their latter use allowed to notably increase the inherent J-V properties, leading to a considerable enhancement in the overall photovoltaic output. The power conversion efficiency of the optimized multilayer BHJ solar cell reached 4.80%, revealing a higher efficiency than the reference cell (3.66%).

Keywords: water-soluble polymer; polythiophene derivative; bulk heterojunction; organic photovoltaic; interfacial layer.

1. Introduction

Significant progress in the field of organic materials for electronic applications has been recently achieved by developing processable and conducting polymers. π-Conjugated polymers (CPs), characterized by a backbone with a delocalized electronic structure, are interesting materials which combine semiconducting properties with light-harvesting features, making them important components for optoelectronic devices, such as light-emitting diodes, field effect transistor and photovoltaic cells [1]. Moreover, although the photovoltaic electricity production is actually dominated by silicon technology, organic solar cells (OSCs) present some potential advantages over the most employed technology, such as light weight, flexibility and the possibility to fine-tune the optoelectronic properties by simply acting on the organic active material structure [2]. Currently,

the most successful approach to build high-performance polymeric OSCs is the donor-acceptor bulk-heterojunction (BHJ) architecture. The photoactive layer of the cell is made of an intimate mixture of an electron-donor (ED) material (the semiconducting conjugated polymer, such as poly(3-hexylthiophene) (PT6H)) and a fullerene derivative (usually [6,6]-phenyl-C_{61}-butyric acid methyl ester, $PC_{61}BM$) acting as an electron-acceptor (EA). Both the components are deposited from a mixed solution using common organic solvents (generally chloroform or chlorobenzene) [3].

The photoactive layer is deposited over a wide range of substrates using solution-based methods, including printing techniques, spin-casting, roll-to-roll technology making the usage of these organic materials more and more cost-effective [4]. Recently, a 9.2 % of photoconversion efficiency (PCE) has been obtained with a polymeric solar cell based on a fluorinated polythiophene derivative, making OSCs more competitive and performing for the rolling out of organic photovoltaic (OPV) technology in the wider mass market [5].

However, the production of OSCs by the current fabrication processes requires the consumption of large amounts of toxic chlorinated or aromatic organic solvents and some efforts have been made towards the study of large-scale environmentally friendly techniques involving the use of water-soluble conjugated polymers (WCPs) as photoactive components in the solar cells [6]. WCPs are generally composed of two main components: π-conjugated backbones and surfactant-like side chain substituents (i. e. amino, phosphate, carboxyl, sulfonic groups) that enhance the polymer solubility in polar solvents. WCPs have also been successfully employed to optimize both organic light-emitting diodes (OLEDs) and OPV devices by fabricating multilayer solar cells in which the water-soluble polymer can act as an electron-collection layer (ECL) or a hole-collection layer (HCL) which improves the electron (hole) extraction and collection to the electrode [7,8]. It has been reported [9] that a thin film of an ECL polymer interposed between the photoactive blend and the Al electrode was able to double the efficiency of a PT6H:$PC_{61}BM$ BHJ solar cell by restraining the penetration of Al atoms into the active layer. Moreover, the use of a thin layer of a cationic conjugated polymer between the active layer and the metal electrode can effectively increase the PCE of the solar cell, since the WCP is able, at the same time, to selectively transport electrons (while simultaneously blocking positive holes) and to suppress the diffusion and reaction between the metal electrode and the active layer components, acting as a chemical buffer layer [10,11]. On the other hand, interfacial optimization at the hole-collection electrode (HCE), usually ITO, has the same importance as that at the electron-collection electrode (ECE) in organic solar cell applications. Nowadays, PEDOT-PSS is the most employed HCL but it shows some drawbacks, since it is a composite material with a large ratio of non-conjugated polymer [6] and has a marked tendency to give inhomogeneous films especially when deposited from its concentrated solutions. Anionic conjugated polymers such as sulfonate-substituted polytriphenylamine [12] and poly(vinylcarbazole) sulfonate lithium salt [13] have been reported as efficient substitute of commonly used PEDOT-PSS. In addition, the high solubility of WCPs in highly polar solvents is particularly suitable for fabricating multilayer devices without interface mixing through the deposition of different layers from orthogonal solvents [14] in order to preserve the chemical and morphological integrity of any single layer.

In this study, we wish to report the synthesis and characterization of two water-soluble polythiophenic polymers: poly{3-[(6-sodium sulfonate)hexyl]thiophene} (PT6S, Scheme 1) and

poly{3-[(6-trimethylammoniumbromide)hexyl]thiophene} (PT6N) prepared through an efficient and straightforward procedure based on the post-functionalization of a regioregular polymeric precursor. Both the synthesized polymers have been completely characterized using spectrochemical and morphological analysis and used either as active-layer or interface layer materials in polymeric solar cells with a BHJ architecture.

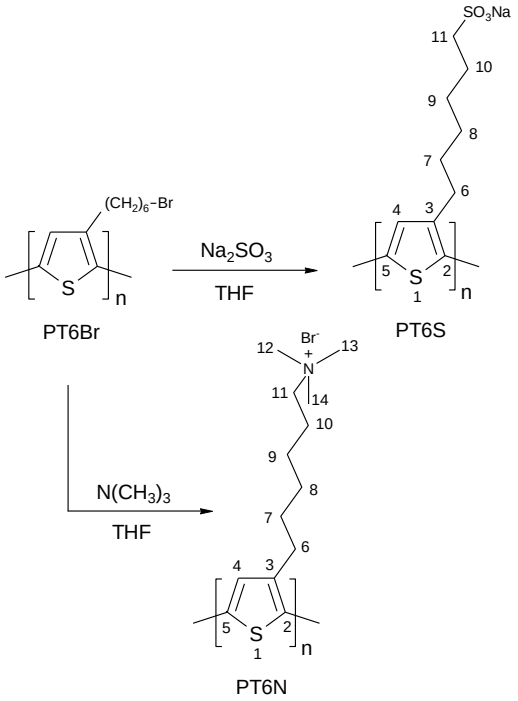

Scheme 1. Synthesis of PT6S and PT6N

2. Experimental

2.1. Materials

All reagents were purchased from Sigma-Aldrich Chemical Co. and used without further purification where not expressly indicated otherwise. All solvents used (HPLC grade) were dried and purified by normal laboratory procedures, stored over molecular sieves and handled in a moisture-free atmosphere.

The reference polymer for OSCs, that is, poly(3-hexylthiophene) (PT6H, HT dyads: 97%, Mn: 25.800 g/mol; PDI: 1.18), was synthesized according to Ref. [15].

2.2. Instrumentation

^{1}H- and ^{13}C-NMR were recorded on a Varian Mercury 400 spectrometer (400 MHz) using TMS as a reference. IR spectra were taken on KBr disks using a Perkin Elmer Spectrum One spectrophotometer. UV-Vis spectra were recorded on a Perkin Elmer Lambda 19 spectrophotometer

using 10^{-5} M polymer solutions in spectroquality solvents in Suprasil quartz cuvettes (1 cm × 1 cm) or films on quartz slides. Molecular weights were determined by gel permeation chromatography (GPC) by using THF solutions on a Linear Instruments UVIS-200 apparatus operating at 254 nm, equipped with a Phenomenex Mixed bed column 5μ MXL type. The calibration curve was recorded using monodisperse polystyrene standards. Cyclic voltammetry (CV) measurements were made using a Pt electrode coated with a thin film of polymer deposed by casting from a water solution, by means of a single compartment three electrodes cell in acetonitrile solution with nBu_4NBF_4 0.1 M as supporting electrolyte. The working electrode was a Pt disk, the counter electrode a Pt wire and the reference an aqueous saturated calomel electrode (SCE). The data were collected by an Autolab PGSTAT20 (Ecochemie, Utrecht, The Netherlands) potentiostat/galvanostat at a potential scan rate of 100 mV/s.

A DSC TA Instruments 2920 was used for the thermal analysis by varying the temperature from -50°C to 250°C at a rate of 5°C min^{-1} in a nitrogen atmosphere. A TGA TA Instruments 2050, operating under inert atmosphere, was used to determine the decomposition temperatures of the samples by heating from 30°C to 900°C at a scan rate of 10°C min^{-1}. Elemental analysis was performed by Redox Laboratories Srl, Monza, Italy. SEM characterizations were carried out on a Phenom World ProX electronic microscope.

BHJ solar cells were prepared according to the following procedure: the ITO glass substrate (1 cm × 1 cm, surface resistance 20 Ω/sq) was etched on one side by using a 10% wt aqueous solution of HCl and heated at 60°C for 15 min in order to obtain an area of 1.5 × 1 cm covered by indium tin oxide. The glass was then cleaned in an ultrasonic bath (Elmasonic S30H) using acetone and then treated at 60°C for 20 min with a solution of aqueous NH_3 (0.8 M) and H_2O_2 (0.5 M), rinsed with distilled water, 2-propanol and dried with a nitrogen flow. The final resistance of the ITO glass was 12 Ω/sq. Poly(3,4-ethylenedioxythiophene):polystyrene sulfonic acid (PEDOT:PSS, 2.8 wt% dispersion in water, viscosity 20 cps) was diluted 1:1 v/v with 2-propanol, sonicated, filtered on a Gooch G2 and the resulting solution (viscosity 12 cps) deposited over the previously treated ITO glass by the doctor blading technique using a Sheen Instrument Model S265674, leaving only a small (0.5 × 0.5 cm) area uncovered at the opposite side of the previously etched area. The PEDOT:PSS film was heated in a Büchi GKR-50 glass oven at 130°C for 2 h under vacuum (10^{-3} mmHg). A solution made by mixing 10 mg of polymer (PT6S, PT6N or the reference polymer PT6H), 10 mg of [6,6-phenyl-C_{61}-butyric acid methyl ester] (PCBM, SES Research, Texas, USA) in 1.5 ml of water (chlorobenzene for PT6H) was sonicated for 15 min, filtered on a PTFE septum (0.45 μm pore size) and deposited by doctor blading on the slide in order to cover the PEDOT:PSS layer. The sample was then annealed in the glass oven under vacuum (10^{-3} mmHg) at 120°C for 15 min. Finally, a 50 nm thick Al electrode was deposited over the polymeric layer through a shadow mask using an Edwards 6306A coating system operating at 10^{-6} mmHg. The active area of the cell was 0.25 × 0.25 cm^2. The deposition of the ECL/HCL layers have been made by means of a BLE 3000 spin coater operating at 1500 rpm using diluted water solutions (ca. 10^{-6} M) of PT6N and PT6S. The solution of the latter polymer was acidified up to pH 1 with H_2SO_4 before deposition. All the prepared cells were subjected to the annealing procedure before the deposition of the Al cathode. The current-voltage characteristics were measured using a Keithley 2401 source meter under the illumination of an Abet Technologies LS150 Xenon Arc Lamp Source AM 1.5 Solar Simulator (100 mW/cm^2) calibrated with an ILT 1400-BL photometer. The structure of the single

layer (SL) devices were: ITO (80 nm)/PEDOT:PSS (120 nm)/active layer (polymer-PCBM 1:1 w/w, 150 nm)/Al (50 nm). The multilayer (ML) cells, with the charge-transport layers, had the following architectures: ML1 [ITO (80 nm)/PT6S (20 nm)/PT6H-PCBM 1:1 w/w (150 nm)/Al (50 nm)]; ML2 [ITO (80 nm)/PEDOT:PSS (120 nm)/PT6H-PCBM 1:1 w/w (150 nm)/PT6N (10 nm)/Al (50 nm)] and ML3 [ITO (80 nm)/PT6S (20 nm)/PT6H-PCBM 1:1 w/w (150 nm)/PT6N (10 nm)/Al (50 nm)]. Layer thicknesses were measured using a Film Thickness Probe FTPAdvances FTPadv-2 (Sentech GmbH, Germany) equipped with the FTPExpert software. This apparatus was previously calibrated with polymer samples of known thicknesses as measured by means of a Burleigh Vista 100 AFM operating in a non-contact tapping mode. The spectral response of the solar cells was measured using a SCSpecIII (SevenStar Optics, Beijing, PRC) incident photon to charge carrier efficiency.

2.3. Polymer synthesis

2.3.1. Poly{3-[(6-sodium sulfonate)hexyl]thiophene} (PT6S)

0.219 g (0.90 mmol) of poly[3-(6-bromohexyl)thiophene] (PT6Br, HT dyads: 94%, Mn: 25500 g/mol; PDI: 1.16), prepared following the procedure described in Ref. [16], in 20 ml of anhydrous THF was added to 0.125 g (0.99 mmol) of Na_2SO_3. The mixture was refluxed for 72 h under stirring. The solvent was evaporated at reduced pressure and the obtained polymer was poured in a glass Gooch filter crucible (G3) and washed several times with methanol giving 0.192 g (0.72 mmol) of PT6S (80% yield).

^{1}H-NMR (D_2O/d_8THF 9:1 v/v, ppm): δ 7.00 (1H, s, H4); 3.42 (2H, t, H11); 2.81 (2H, t, H6); 1.85 (2H, m, H10); 1.74 (2H, m, H9); 1.48 (4H, m, H7+H8).

^{13}C-NMR (D_2O/d_8THF 9:1 v/v, ppm): δ 139.72 (C3); 134.15 (C4); 124.98 (C5); 123.36 (C2); 39.05 (C11); 31.87 (C6); 29.65 (C7); 28.62 (C8); 27.18 (C9); 26.42 (C10).

FT-IR (KBr, cm^{-1}): 3028 (ν C-H (β-thiophene)), 2928 (ν_{as} C-H (–CH_2-)), 2853 (ν_s C-H (–CH_2-)), 1573 (ν_{as} C=C (thiophene)), 1418 (ν_s C=C (thiophene)), 1136 (ν -SO_3^-) , 817 (γ C-H (2,3,5-trisubstituted thiophene)), 719 (–CH_2- rocking).

Elemental analysis: Calcd. for $[(C_{10}H_{13}O_3S_2Na)]_n$: C 44.76; H 4.88; O 17.89; S 23.90; Na 8.57. Found: C 44.81; H 4.93; O 17.92; S 23.95; Na 8.39.

2.3.2. Poly{3-[(6-N,N,N-trimethylammoniumbromide)hexyl]thiophene} (PT6N)

0.253 g (1.04 mmol) of PT6Br in 20 ml of anhydrous THF was cooled down to -78°C and added with 5.00 g (85 mmol) of N,N,N-trimethylamine. The mixture was stirred for 2h at -78°C under an inert atmosphere and then stirred for further 24 h at room temperature. The solvent was removed at reduced pressure and the obtained polymer was poured in a glass Gooch filter crucible (G3) and washed several times with methanol giving 0.234 g (0.76 mmol) of PT6N (74% yield).

^{1}H-NMR (D_2O, ppm): δ 6.99 (1H, s, H4); 3.45 (2H, t, H11); 3.12 (9H, s, H12+H13+H14); 2.83 (2H, t, H6); 1.87 (2H, m, H10); 1.76 (2H, m, H9); 1.48 (4H, m, H7+H8).

^{13}C-NMR (D_2O, ppm): δ 139.75 (C3); 134.17 (C4); 124.99 (C5); 123.38 (C2); 59.27 (C11); 52.35 (C12+C13+C14); 29.89 (C6); 27.54 (C7); 27.24 (C8); 24.12 (C9); 24.11 (C10).

FT-IR (KBr, cm^{-1}): 3029 (ν C-H (β-thiophene)), 2930 (ν_{as} C-H ($–CH_2$- + -CH_3)), 2870 (ν_s C-H ($–CH_2$-)), 2835 (ν_s C-H ($–CH_3$)), 1510 (ν_{as} C=C (thiophene)), 1464 (ν_s C=C (thiophene)), 1418 ($–CH_3$ deformation), 1050 (ν C-N) , 840 (γ C-H (2,3,5-trisubstituted thiophene)), 720 ($–CH_2$- rocking).

Elemental analysis: Calcd. for $[(C_{13}H_{22}NSBr)]_n$: C 51.31; H 7.29; N 4.60; S 10.54; Br 26.26. Found: C 51.38; H 7.19; N 4.65; S 10.66; Br 26.12.

3. Results and Discussion

The synthesis of water-soluble regioregular poly{3-[(6-sodium sulfonate)hexyl]thiophene} (PT6S) and poly{3-[(6-N,N,N-trimethylammoniumbromide)hexyl]thiophene} (PT6N) is shown in Scheme 1. For the preparation of the anionic polymer PT6S, the side-chain bromine atom in the regioregular precursor poly[3-(6-bromohexyl)thiophene] (PT6Br) was subjected to SN2 reaction with sodium sulfite. The obtained dark-orange polymer was soluble in water (10 mg/ml) and in THF (up to 18 mg/ml).

The formation of water-soluble cationic PT6N was achieved in high yields through the quaternization of PT6Br with trimethylamine in THF operating at low temperature (-78°C) and the final product resulted highly soluble in water (up to 17 mg/ml), but only partially soluble in THF (2 mg/ml). Both the polymers were insoluble in methanol and ethanol and their characteristics are reported in Table 1.

The molecular weights were determined by GPC using THF as eluent. PT6S showed a number average molecular weight value which is in good agreement with its precursor PT6Br, while the M_n value of the aminic-functionalized polymer was notably lower. This can be related to the scarce solubility of PT6N in THF which prevented the analysis of the whole polymeric sample, since the polymer solutions were filtered through a PTFE septum (0.20 μm pore size) before being injected in the GPC system.

The FT-IR main bands of PT6S and PT6N are reported in the Experimental section and their spectra are shown in Fig. 1.

Both the spectra show the complete disappearance of the band at 647 cm^{-1} (aliphatic C-Br stretching) and the appearance of new absorptions ascribable to the sulfonate (1136 cm^{-1}) and trimethylaminic (2835, 1418 and 1050 cm^{-1}) moieties, respectively, clearly indicating the quantitative substitution of halogen in the precursor polymer.

Table 1. Structural characteristics of the synthesized polymers

	PT6S	PT6N
Yield (%)[a]	80	74
M_n (g/mol)[b]	24300	19000
M_w/M_n[c]	1.18	1.12
DP_n[d]	80	56
HT (%)[f]	92	92

[a] Post-functionalization yield

[b] Number average molecular weight

[c] Polydispersity index

[d] Polymerization degree

[f] Head-to-tail dyads percentage

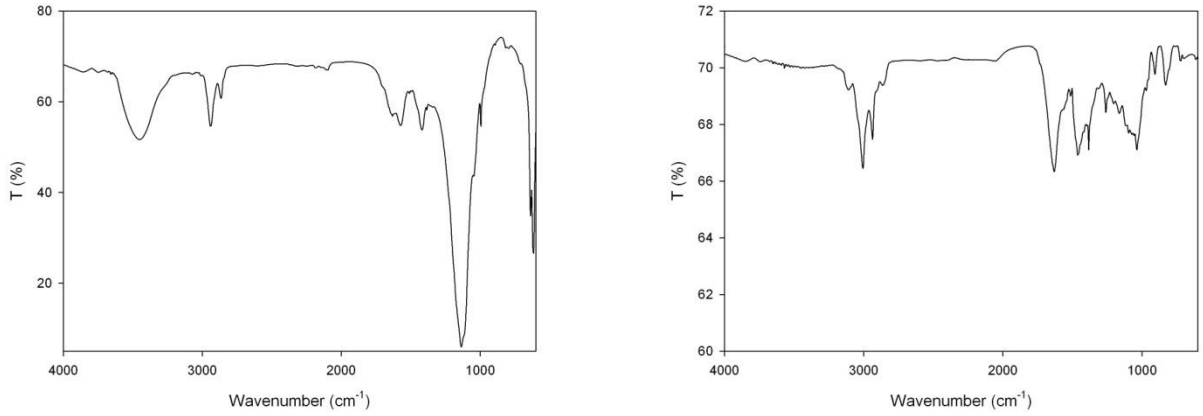

Fig. 1. FT-IR spectra of PT6S (left) and PT6N (right)

This result is confirmed also by the NMR analysis, since in both the samples the signals of the inserted groups are clearly evident. In fact, the ^{1}H-NMR spectrum of PT6S (Fig. 2) shows the triplet ascribable to the methylenic protons α- to the sulfonic group at 3.42 ppm, and in the spectrum of PT6N the signals due to the aminic functionality appear at 3.45 and 3.12 ppm (methylenic protons of the alkylic chain α- to the $N(CH_3)_3$ group and methylic protons of the quaternary amine, respectively). The ^{13}C-NMR spectra (Fig. 3) are also in good agreement with the expected polymer structure showing, in PT6S, the α-C to sulfonic group at 39.05 ppm and, in PT6N, the α-C to

$N(CH_3)_3$ group at 59.27 and the methylic carbons at 52.35 ppm. The elemental analyses further confirm the proposed structures (see Experimental section).

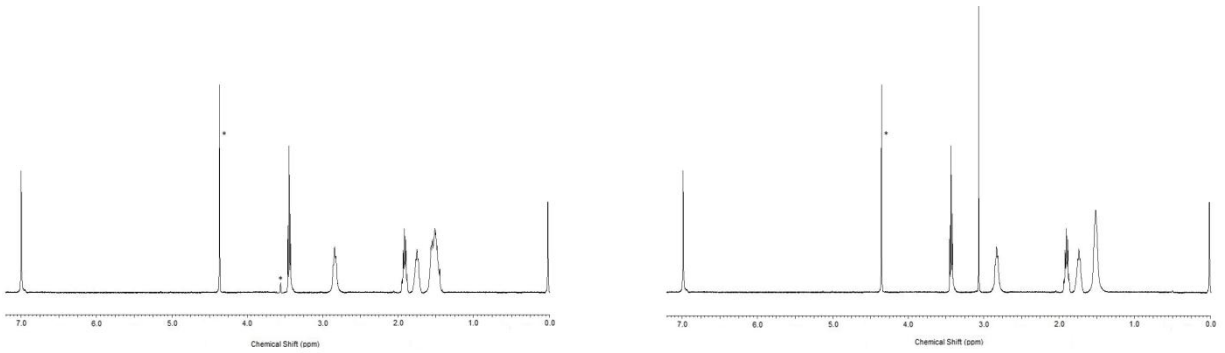

Fig. 2. ^{1}H-NMR spectra of PT6S in D_2O/d_8THF 9:1 v/v (left) and PT6N in D_2O (right). Asterisk: solvent resonance

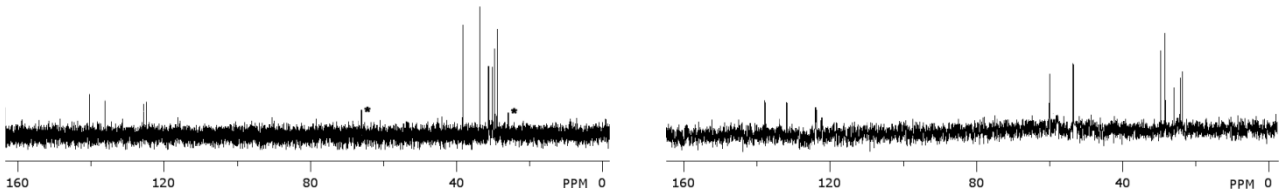

Fig. 3. ^{13}C-NMR spectra of PT6S in D_2O/d_8THF 9:1 v/v (left) and PT6N in D_2O (right). Asterisk: solvent resonance

The DSC thermograms of PT6S and PT6N are shown in Fig. 4 and the main thermal transitions values reported in Table 2.

The thermal behavior of the two polymers is quite different. PT6S shows a T_g lower than PT6N that can be ascribed to the longer side chain of the former (11.11 vs 10.15 Å, as calculated from density functional theory (DFT) for the B3LYP/6-31G(d) level). In fact, longer chains or more sterically-demanding groups provide a higher free-volume, permitting the molecular chains to move more easily, thus lowering T_g [17].

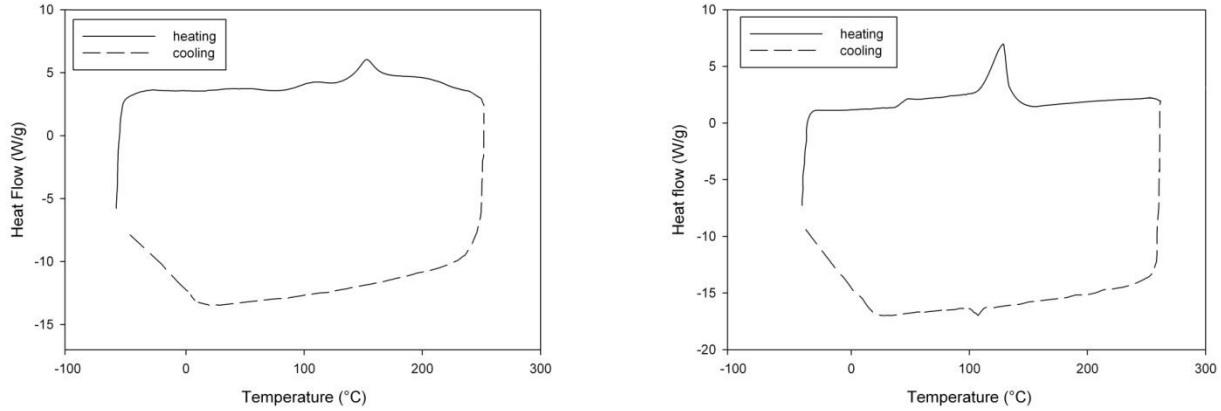

Fig. 4. DSC thermograms of PT6S (left) and PT6N (right). The curves refer to the second scan and were recorded under nitrogen at a heating/cooling rate of 5°C/min.

Table 2. Thermal characteristics[a] of polymer samples

Sample	T_g (°C)	T_{m1} (°C)	T_{m2} (°C)	T_c (°C)	ΔH_{m1} (J/g)	ΔH_{m2} (J/g)	ΔH_c (J/g)	T_d (°C)
PT6S	45	91	139	-	0.7	3.9	-	350
PT6N	55	-	129	111	-	17.8	3.7	270

[a] T_g = glass-transition temperature; T_m = melting temperature; T_c = crystallization temperature ; T_d = decomposition temperature

Moreover, PT6S shows two melting temperatures, at 91 and 139°C, ascribable to the melting of the side chain and main chain, respectively, while PT6N clearly evidences only the first-order transition due to the backbone melting, together with the crystallization temperature and an higher value of ΔH_m.

The TGA thermograms of the two polymers under nitrogen at a heating rate of 10°C/min are reported in Fig. 5. As seen in the TGA curves in Fig. 5, PT6N shows a two-step weight loss process with onset temperature (T_d) at about 270°C. The first weight loss increases rapidly from the onset temperature up to about 370°C and the second increases less rapidly up to about 520°C. The derivative TG curve exhibits degradation peaks centered at 325°C for the first loss range and 431°C for the second. The first weight loss seems consistent with a partial cracking of the aminic functionality associated with the loss of methyl groups. By contrast, PT6S shows only a single-step weight loss, starting at about 350°C with a degradation peak centered at 408°C. It is important to underline that the thermal degradation behavior of the samples is almost the same in air, showing only a slight decrease of the T_d values (6°C for PT6N and 4°C for PT6S). The high decomposition temperatures of both the samples make them appropriate for integration into OSCs.

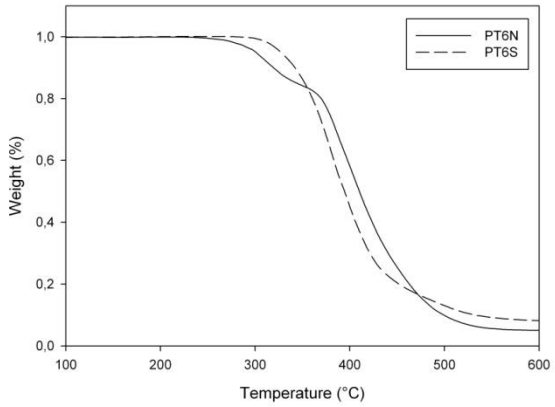

Fig. 5. TGA thermograms of the two polymers recorded under nitrogen at a heating rate of 10°C/min.

The high solubility of the two polymers in water made it possible to perform their UV-Vis spectra in this solvent. Fig. 6 shows the solvatochromic behavior of PT6S and PT6N at increasing non-solvent (methanol) molar fractions.

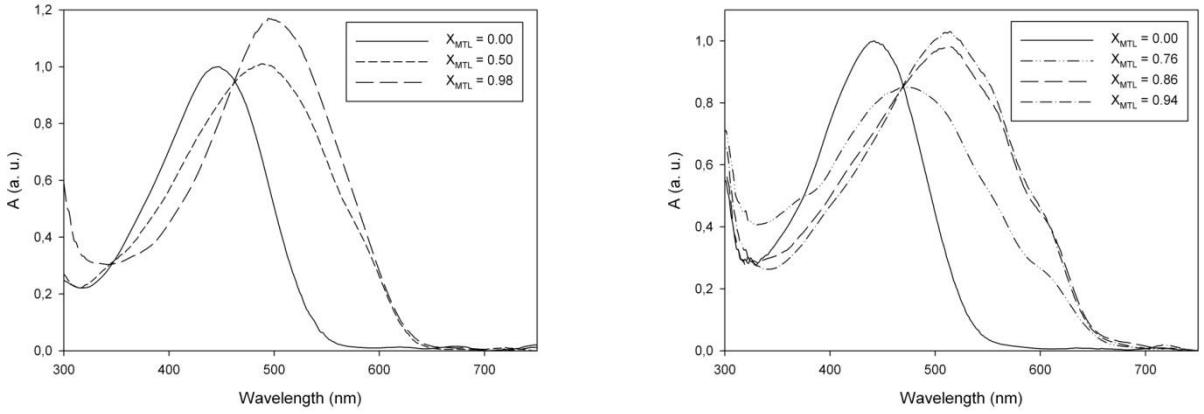

Fig. 6. Solvatochromism of PT6S (left) and PT6N (right) in H_2O/CH_3OH at increasing methanol molar fractions.

For both the polymers, the addition of methanol to their aqueous solutions shows a transformation from the more solvated (less ordered) to the less solvated (more conjugated) conformation [18]. The presence of an evident isosbestic point confirms the existence of two distinct chromophores in the examined solutions. The solvatochromic transition is clearly visible as a marked solution color change from yellow-orange to dark red, without any trace of macroscopic aggregation being detected, at the adopted concentration (about 10^{-5} M), even after many days. The non-solvent effect is more evident for PT6N ($\Delta\lambda_{max}$ = 75 nm, from 440 to 515 nm) than for PT6S ($\Delta\lambda_{max}$ = 57 nm, from 446 to 503 nm) and the spectrum of the former also shows vibronic sidebands at 552 and 608 nm at higher non-solvent concentrations.

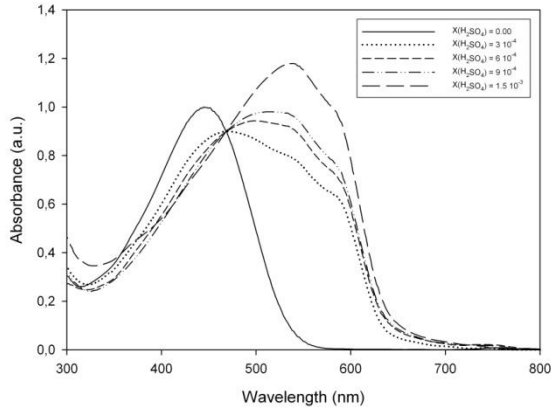

Fig. 7. Solvatochromism of PT6S in H_2O/ H_2SO_4 at increasing sulfuric acid molar fractions.

The presence of these absorptions indicates that PT6N chains can assume highly planar conformations, giving rise to enhanced electronic and optical properties [19].

Moreover, while the aqueous solution of PT6N is almost insensitive to pH variations, PT6S shows an evident chromism in H_2O/H_2SO_4 solution, even at low acid molar fractions (Fig. 7). In this case, the absorption maximum undergoes a red-shift of 89 nm (from 444 to 533 nm) passing from pH = 6.8 (pure water) to pH = 0.8 ($1.5\ 10^{-3}$ H_2SO_4 molar fraction). Progressive additions of sulfuric acid causes also the appearance of the $E_{0\text{-}0}$ (pure electronic transition) visible in the UV-Vis spectrum as a shoulder at 591 nm. Higher acid concentrations lead to the protic doping of the polythiophenic backbone, with the evident appearance of an absorption centered at 753 nm (polaronic band).

The UV-Vis spectra of PT6S and PT6N were also recorded in the solid state, on a thin polymer film on quartz slides. Their spectra are reported in Fig. 8, together with the spectrum of the reference polymer PT6H (see Experimental section). Contrary to the solution state, PT6S spectrum does not show any evident vibronic substructure while PT6N shows a weak shoulder at about 580 nm and PT6H two evident vibronic quanta at 545 and 604 nm. The measured absorption maxima (λ_{max}) of the three samples are: 491 nm (PT6S), 524 nm (PT6N) and 511 nm (PT6H), corresponding to an average conjugation length (n_L) of 10, 15 and 12 thiophenic rings, respectively [20]. When cast from an aqueous acid solution, the spectrum of PT6S in film (Fig. 8) is notably different from the neutral water-cast counterpart, with a λ_{max} shifting from 491 to 497 nm and the appearance of bands ascribable to the π-stacking among polymeric chains at 542 and 581 nm. These absorptions are characteristic of additional electronic transitions as the result of increased molecular ordering [21].

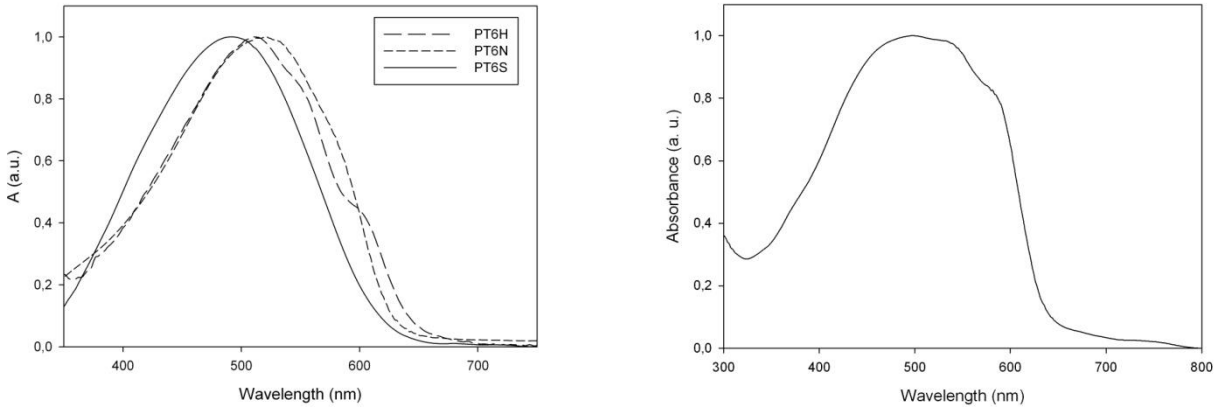

Fig. 8. Left: UV-Vis spectra of polymers in film cast from water (PT6N and PT6S) and $CHCl_3$ (PT6H) solutions. Right: UV-Vis spectrum of PT6S in film cast from H_2O/H_2SO_4 solution (pH ≈1).

Both PT6S and PT6N, submitted to cyclic voltammetry (CV), displayed oxidation and reduction onsets at different potential values ($E_{ox\ onset}$ = 0.48 and 0.63 V; $E_{red\ onset}$ = -1.18 and -1.20 V, respectively). CV curves are reported in Fig. 9.

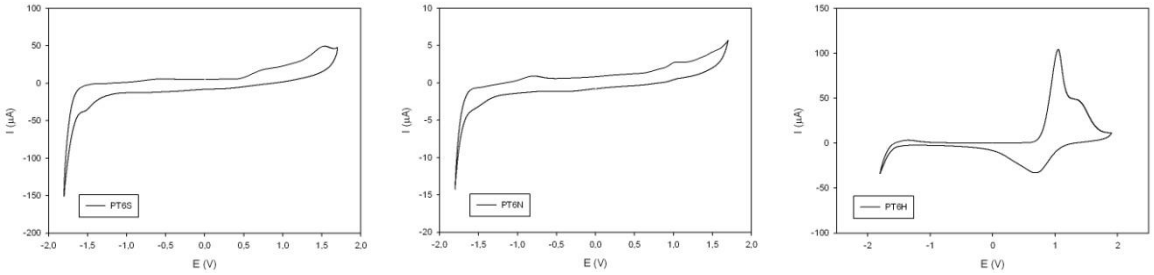

Fig. 9. Cyclic voltammograms of the polymer films on Pt recorded in 0.1 M nBu_4NBF_4 acetonitrile solution at a scan rate of 100 mV/s.

The above potential values displayed by CV curves allowed to directly calculate the highest occupied molecular orbital (HOMO) and the lowest unoccupied molecular orbital (LUMO) energy levels of both the samples, taking into account that the SCE reference electrode has a potential of 4.40 eV relative to vacuum [22]. The obtained values are reported in Table 3 together with the electrochemical bandgap ($E_{g,ec}$).

Since the low electron affinity of the reference polymer forced its reduction potential out of the electrochemical potential window of CH_3CN [23], PT6H did not show any evident reduction peak in the scanned range. Its LUMO energy value was then calculated indirectly, by considering that it corresponds to the HOMO energy plus the optical energy gap evaluated from the onset of the UV-Vis spectrum of the polymer in film (656 nm, 1.89 eV) [24]. It is worth noting that the $E_{g,opt}$ obtained using onset values from absorption spectra in Fig. 8 (630 nm, 1.97 eV for PT6S and 617 nm, 2.01 eV for PT6N) were notably higher than the corresponding values obtained using the onset potentials determined by CV.

Table 3. Electrochemical properties of the polymer films

Polymer	E_{ox} (V)	E_{red} (V)	E_{HOMO} (eV)	E_{LUMO} (eV)	$E_{g,ec}$ (eV)
PT6S[a]	0.48	-1.18	-4.88	-3.22	1.66
PT6N[a]	0.63	-1.20	-5.03	-3.20	1.83
PT6H[b]	0.80	-	-5.20	-3.31	1.89

a) film cast from H_2O solution; b) film cast from $CHCl_3$ solution

This observation is in agreement with Eckardt et al. [25], who stated that when thienylene-based polymers (and not oligomers) were examined, the $E_{g,ec}$ was about 0.16 eV lower than $E_{g,opt}$. This discrepancy was attributed to the broader polydispersity usually occurring in polymeric materials (with respect to the oligomeric ones), leading to the presence of different conjugation lengths in the examined material. Consequently, the lower electrochemical value was adopted as a representative band gap energy at infinite chain length [26]. Anyway, the study of the optical and electrochemical properties of the electron-donor material is of utmost importance, since broader absorption and a lower bandgap energy usually improve the light absorption efficiency, leading to the generation of higher photocurrents.

We have prepared some Single Layer (SL) BHJ solar cells in which the WCPs were used as active components of the blend. Fig. 10 shows the J-V characteristic curves of solar cells having the structure: ITO (80 nm)/PEDOT:PSS (120 nm)/active layer (150 nm)/Al (50 nm) and an active area of 6.25 mm^2 under AM 1.5 irradiation with an intensity of 1 sun (100 mW/cm^2) from a calibrated solar simulator. The operational procedures followed for the preparation of cells are described in the experimental section.

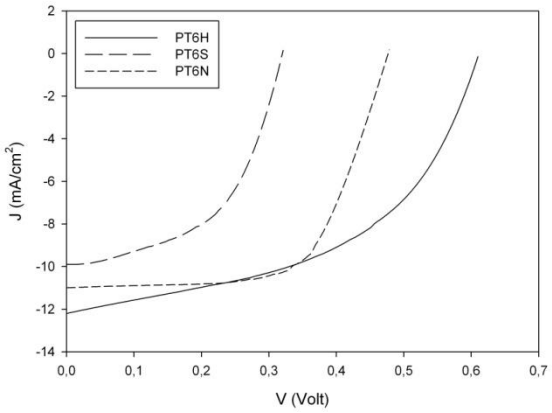

Fig. 10. Current density-voltage for the single-layer tested cells under AM 1.5 one-sun illumination. The curves related to the most performing cells are reported.

The reported PCE values (Table 4) were obtained by measuring five different devices prepared using the same operative conditions.

Table 4. Photovoltaic parameters of SL BHJ solar cells

Sample	J_{sc} (mA cm^{-2})	V_{oc} (V)	FF (%)	PCE_{max} (PCE_{ave}) (%)
PT6H	12.2	0.61	49.2	3.66 (3.41)
PT6S	9.91	0.32	50.3	1.60 (1.48)
PT6N	11.1	0.48	55.1	2.94 (2.82)

The values of open circuit voltage can be also calculated by means of the following relation, where ΔE is the total energy loss in plastic solar cell, which is the sum of the energy losses due to photoinduced electron transfer and the energy loss due to quasi-Fermi level splitting [27]:

$$V_{oc} = \frac{1}{e}\left|E_{donor}HOMO\right| - \left|E_{acceptor}LUMO\right| - \Delta E \quad (1)$$

ΔE can be estimated using V_{oc} and energy levels values of the reference polymer PT6H and E_{LUMO} of PCBM (-3.75 eV), giving a value of 0.84 V. From equation 1, the V_{oc} of PT6S and PT6N are 0.29 and 0.44 V respectively, in good agreement with the measured values. Moreover, the short circuit current J_{sc} is proportional to the amount of light absorbed in the active layer. The incident photon to current efficiency (IPCE) curves, showing the effectiveness of the polymer/PCBM active layers at varying wavelengths, is given in Fig. 11. The normalized integrated intensities were 1 (PT6H), 0.88 (PT6N) and 0.79 (PT6S), which were quite consistent with the J_{sc} ratios (1:0.91:0.81, respectively). Probably, the incorporation of a substituent at the end of the side chains increased the steric bulk of the pendant units, leading to a less planar polythiophenic backbone and then to shorter absoption onsets.

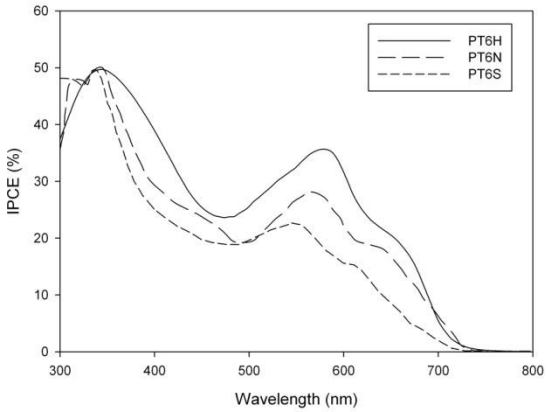

Fig. 11. IPCE (%) spectra of PT6S, PT6N and the reference polymer PT6H blends.

The photovoltaic performances obtained with WCP polymers are lower than that of the reference cell, which was prepared with the same experimental conditions using the PT6H as the electron-donor polymer. This fact can be ascribed to the presence of the polar groups in the chemical structure of WCP which are, on the one hand, responsible of their solubility in aqueous media but, on the other, when used for the preparation of the photoactive blend, can act as exciton-quenching centers and charge carrier trapping points, leading to poorer performances [28-31].

We have then prepared some multilayer (ML) cells with the following architecture: ML1 [ITO (80 nm)/PT6S (20 nm)/PT6H-PCBM 1:1 w/w (150 nm)/Al (50 nm)]; ML2 [ITO (80 nm)/PEDOT:PSS (120 nm)/PT6H-PCBM 1:1 w/w (150 nm)/PT6N (10 nm)/Al (50 nm)] and ML3 [ITO (80 nm)/PT6S (20 nm)/PT6H-PCBM 1:1 w/w (150 nm)/PT6N (10 nm)/Al (50 nm)]. The ECL/HCL layers have been deposited from diluted aqueous solution using the spin-coating technique as described in the Experimental section. PT6S layer was deposited from a H_2O/H_2SO_4 solution (pH $\approx$1) in order to exploit its increased molecular ordering when cast from this solvent mixture; since PT6S also shows an extended absorption spectrum when deposited from acidified water, the thickness of the HCL has been carefully optimized. In particular, some multilayer cells having the ML1 architecture have been prepared and the thickness of the PT6S layer was varied acting on the concentration of polymer in the deposited solution. We observed that the effectiveness of the HCL was reduced if its thickness was lower than 10 nm and higher than 30 nm (data not shown) as, in the latter case, the light absorption by the anionic polymer reduced the light exploitable by the photoactive layer, thus reducing the final J_{sc}. The optimal thickness was found around 20 nm.

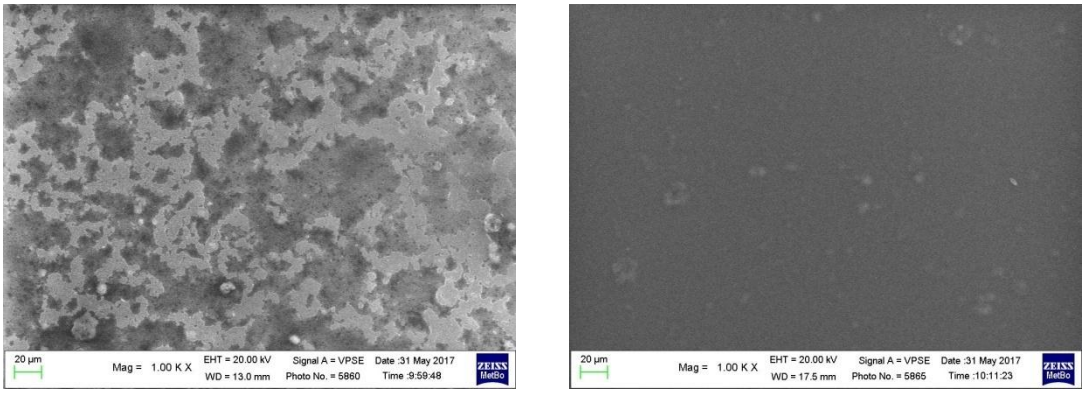

Fig. 12. SEM micrographs of the reference blend before (left) and after (right) the deposition of the PT6N buffer layer.

As for the ECL, the optimum thickness was found around 10 nm, since a thinner layer was ineffective (towards the final efficiency of the cell) while thicker layers gave higher roughness values of the external surface of the device with detrimental effects on cells performance (data not shown). A 10 nm thick layer of PT6N gave a very homogeneous and smooth surface as evidenced by comparing the SEM images of the same cell before and after the application of the buffer layer (Fig. 12). The combined effects of a smoother surface and of intermolecular interactions between

the PT6H donor and the PT6N buffer layer can enhance the contact between the photoactive blend and the Al electrode, enhancing the electron extraction efficiency at the electrode interface [10].

In Table 5 the PCE values for the ML solar cells obtained by measuring five different devices prepared using the same operative conditions are reported. The resulting current density-voltage (J-V) curves are shown in Fig. 13.

Table 5. Photovoltaic parameters of multilayer BHJ solar cells

Architecture	J_{sc} (mA cm^{-2})	V_{oc} (V)	FF (%)	PCE_{max} (PCE_{ave}) (%)
ML1	12.5	0.64	50.2	4.02 (3.91)
ML2	12.4	0.64	48.8	3.88 (3.63)
ML3	13.1	0.65	56.2	4.80 (4.66)

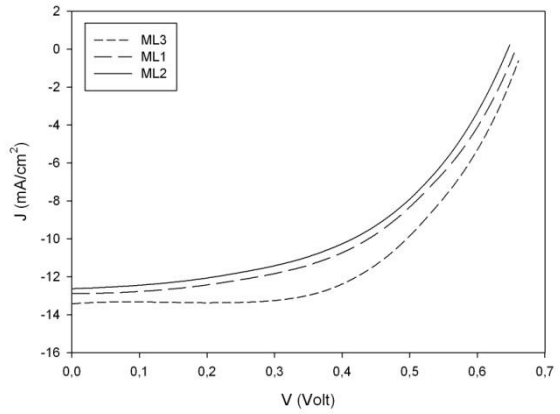

Fig. 13. Current density-voltage for the multilayer cells under AM 1.5 one-sun illumination. The curves related to the most performing cells are reported.

The devices with interfacial charged polymer layers show photovoltaic performances higher than the reference cell, made with the same photoactive layer but devoid of any charge-collection layer, as reported in Table 4 (PT6H). The replacement of PEDOT:PSS with a thin film of PT6S, cast from a H_2O/H_2SO_4 solution, as an HCL in ML1 cell was successful, since the latter polymer can provide better routes for holes transport [32]. In fact, Leclerc et al [33] reported that poly[ω-(thienyl)alkanesulfonate)]s can undergo a partial doping, without the use of any external oxidizing agent, when dissolved in protic acid water solutions. This self-acid-protic reaction leads to stable and highly-conducting materials which can make easier the achievement of more effective percolation paths for the positive holes toward the ITO electrode. Even if the absence of any evident polaronic band in the UV-Vis spectrum of PT6S cast from aqueous acid solution does not evidence the presence of acid-doping of the polymeric backbone (at least at the employed acid concentrations), the appearance of an evident fine structure at lower energies suggests an improved order of the polymer in the solid state, to the benefit of the mean conjugation length and then to the conductivity of the hole collecting layer. Moreover, the PT6S HOMO level (-4.88 eV) is closer to

the ITO workfunction (-4.70 eV) than PEDOT-PSS (-5.0 eV [13]), making the charge transfer to the anode more favorable and implying a nearly ohmic contact for hole injection/transport from the active layer to ITO.

If we compare the PCE of the reference cell (PT6H, Table 4) with ML2 (Table 5) we can observe that the introduction of the ECL produces positive effects on the PCE of the solar cell although in a lesser extent than in the case of PT6S. The (slight) V_{oc} increase of 0.03 V can be the consequence of the vacuum level shift or band bending induced by interfacial dipoles which accumulate near the metal electrode [34,35], that can also lead to a higher electric field across the active layer [36,37]. The best performing cell was obtained by replacing PEDOT/PSS with PT6S and adding a PT6N interlayer between the active blend and the Al electrode (ML3). In this case, the PCE notably increased (from 3.66 to 4.80 %) owing to the simultaneous effects of two types of WCPs.

4. Conclusions

We report the syntheses of two water-soluble regioregular polythiophenic derivatives functionalized at the end of an hexamethylenic side chain with a sulfonate and a trimethylaminic group, respectively. The two conjugated polyelectrolytes (CPE)s have been tested as photoactive components and as interface modification layers in organic solar cells having a bulk heterojunction (BHJ) architecture. The single-layer cells using the water-soluble polymers for the photoactive blend gave photoconversion efficiency values lower than the reference cell made with PT6H cast from a more conventional solvent, indicating that the photovoltaic performances of these polymers still remain lower than their non-water soluble counterparts.

However, the device performance of a conventional solar cell can be remarkably improved by incorporating a thin layer of the suitable CPE as electron-collection layer (ECL) or hole-collection layer (HCL). The best result (+31% if compared with the PCE of the reference cell) was obtained for the multi-layer cell employing a thin layer of HCL instead of the commonly used PEDOT-PSS and a thin layer of ECL between the photoactive layer and the cathode, demonstrating the high effectiveness of CPEs when employed as interface modifiers. These findings open up new design solutions for novel more-performing organic solar cells.

Acknowledgements

The authors are grateful to Prof. Luigi Angiolini of the University of Bologna for helpful discussions about the manuscript.

References

[1] L. Lu, M. A. Kelly, W. You, L. P. Yu, Status and prospects for ternary organic photovoltaics, Nat. Photonics 9 (2015) 491-500.

[2] S. Wen, X. Bao, W. Shen, C. Gu, Z. Du, L. Han, D. Zhu, R. Yang, Benzodithiophene-based poly (aryleneethynylene)s: Synthesis, optical properties, and applications in organic solar cells, J. Polym. Sci, Part A: Polym. Chem., 52 (2014) 208-215.

[3] O. Synooka, F. Kretschmer, M. D. Hager, M. Himmerlich, S. Krischok, D. Gehrig, F. Laquai, U. S. Schubert, G. Gobsch, H. Hoppe, Modification of the active layer/PEDOT: PSS interface by solvent additives resulting in improvement of the performance of organic solar cells, Appl. Mater. Interfaces, 6 (2014) 11068-11081.

[4] J. Szeremeta, M. Nyk, M. Samoc, Photocurrent enhancement in polythiophene doped with silver nanoparticles, Optical materials, 37 (2014) 688-694.

[5] Q. Fan, W. Su, X. Guo, B. Guo, W. Li, Y. Zhang, K. Wang, M. Zhang, Y. Li, A New Polythiophene Derivative for High Efficiency Polymer Solar Cells with PCE over 9%, Adv. Energy Mater. (2016) 1600430.

[6] C. Duan, K. Zhang, C. Zhong, F. Huang, Y. Cao, Recent advances in water/alcohol-soluble π-conjugated materials: new materials and growing applications in solar cells, Chem. Soc. Rev., 42 (2013) 9071-9104.

[7] J. H. Seo, A. Gutacker, Y. M. Sun, H. B. Wu, F. Huang, Y. Cao, U. Scherf, A. J. Heeger, G. C. Bazan, Improved high-efficiency organic solar cells via incorporation of a conjugated polyelectrolyte interlayer, J. Am. Chem. Soc., 133 (2011) 8416-8419.

[8] K. Yao, L. Chen, Y. Chen, F. Li, P. Wang, Influence of water-soluble polythiophene as an interfacial layer on the P3HT/PCBM bulk heterojunction organic photovoltaics, J. Mater. Chem., 21 (2011) 13780-13784.

[9] Y. Zhao, Z. Xie, C. Qin, Y. Qu, Y. Geng, L. Wang, Enhanced charge collection in polymer photovoltaic cells by using an ethanol-soluble conjugated polyfluorene as cathode buffer layer, Sol. Energy Mater. Sol. Cells, 2009 (93) 604-608.

[10] Y.Wang , B. Liu, A. Mikhailovsky, G.C. Bazan, Conjugated polyelectrolyte–Metal nanoparticle platforms for optically amplified DNA detection, Adv. Mater. 22 (2010) 656-659.

[11] F. Zhang, M. Ceder, O. Inganäs, Enhancing the photovoltage of polymer solar cells by using a modified cathode, Adv. Mater., 19 (2007) 1835-1838.

[12] W. Shi, S. Q. Fan, F. Huang, W. Yang, R. S. Liu, Y. Cao, Synthesis of novel triphenylamine-based conjugated polyelectrolytes and their application as hole-transport layers in polymeric light-emitting diodes, J. Mater. Chem., 16 (2006) 2387-2394.

[13] X. Gong, S. Wang, D. Moses, G. C. Bazan, A. J. Heeger, Multilayer polymer light emitting diodes: white-light emission with high efficiency, Adv. Mater., 17 (2005) 2053-2058.

[14] C. M. Zhong, C. H. Duan, F. Huang, H. B. Wu, Y. Cao, Materials and devices toward fully solution processable organic light-emitting diodes, Chem. Mater., 23 (2011) 326-340.

[15] M. Lanzi, E. Salatelli, T. Benelli, D. Caretti, L. Giorgini, F. P. Di-Nicola, A regioregular polythiophene–fullerene for polymeric solar cells, J. Appl. Polym. Sci., 132 (2015) 42121, 1-10.

[16] M. Lanzi, L. Paganin, New regioregular polythiophenes functionalized with sulfur-containing substituents for bulk heterojunction solar cells, React. Funct. Polym., 70 (2010) 346-360.

[17] X. Hu, L. Xu, Structure and properties of 3-alkoxy substituted polythiophene synthesized at low temperature, Polymer, 41 (2000) 9147-9154.

[18] F. Bertinelli, P. Costa Bizzarri, C. Della Casa, M. Lanzi, Analysis of UV–Vis spectral profiles of solvatochromic poly [3-(10-hydroxydecyl)-2, 5-thienylene], Spectrochimica Acta Part A, 58 (2002) 583-592.

[19] K. Sakurai, H. Tachibana, N. Shiga, C. Terakura, M. Matsumoto, Y. Tokura, Experimental determination of excitonic structure in polythiophene, Phys. Rev. B, 56 (1997) 9552-9556.
[20] R. Qian, Aspects of molecular design of conducting polymers, Makromol. Chem., Macromol. Symp. 33 (1990) 327-339.
[21] P. T. Wu, H. Xin, F. S. Kim, G. Ren, S. A. Jenekhe, Regioregular poly (3-pentylthiophene): synthesis, self-assembly of nanowires, high-mobility field-effect transistors, and efficient photovoltaic cells, Macromolecules, 42 (2009) 8817-8826.
[22] J. Pommerehne, H. Westweber, W. Guss, R. F. Mahrt, H. Bassler, M. Porsch, J. Daub, Efficient two layer leds on a polymer blend basis, Adv. Mater. 7 (1995) 551-554.
[23] T. Johansson, W. Mammo, M. Svensson, M. R. Andersson, O. Inganas, Electrochemical bandgaps of substituted polythiophenes, J. Mater. Chem., 13 (2003) 1316-1323.
[24] M. Lanzi, F. P. Di Nicola, F. Errani, L. Paganin, A. Mucci, Solventless deposition of oligo-and polythiophenes for bulk heterojunction solar cells, Synth. Met., 195 (2014) 61-68.
[25] H. Eckhardt, L. W. Shacklette, K. Y. Jen, R. L. Elsenbaumer, The electronic and electrochemical properties of poly (phenylene vinylenes) and poly (thienylene vinylenes): An experimental and theoretical study, J. Chem. Phys., 91 (1989) 1303-1315.
[26] R. Holze, Optical and electrochemical band gaps in mono-, oligo-, and polymeric systems: a critical reassessment, Organometallics, 33 (2014) 5033-5042.
[27] M. C. Scharber, D. Muehlbacher, M. Koppe, P. Denk, C. Waldauf, A. J. Heeger, C. J. Brabec, Design rules for donors in bulk-heterojunction solar cells—Towards 10% energy conversion efficiency, Adv. Mater. 18 (2006) 789-794.
[28] J. H. Yang, A. Garcia, T. Q. Nguyen, Organic solar cells from water-soluble poly(thiophene)/fullerene heterojunction, Appl. Phys. Lett., 90 (2007) 103514.
[29] R. Søndergaard, M. Helgesen, M. Jørgensen, F. C. Krebs, Fabrication of polymer solar cells using aqueous processing for all layers including the metal back electrode, Adv. Energy Mater., 1 (2011) 68-71.
[30] B. J. Worfolk, D. A. Rider, A. L. Elias, M. Thomas, K. D. Harris, J. M. Buriak, Bulk heterojunction organic photovoltaics based on carboxylated polythiophenes and PCBM on glass and plastic substrates, Adv. Funct. Mater., 21 (2011) 1816-1826.
[31] J. Vandenbergh, J. Dergent, B. Conings, T. Krishna, W. Maes, T. J. Cleij, L. Lutsen, J. Manca, D. J. Vanderzande, Synthesis and characterization of water-soluble poly (p-phenylene vinylene) derivatives via the dithiocarbamate precursor route, Eur. Polym. J. 47 (2011) 1827-1835.
[32] W. Li, B. J. Worfolk, P. Li, T. C. Hauger, K. D. Harris, J. M. Buriak, Self-assembly of carboxylated polythiophene nanowires for improved bulk heterojunction morphology in polymer solar cells, J. Mater. Chem., 22 (2012) 11354.
[33] M. Chayer, K. Faid, M. Leclerc, Highly conducting water-soluble polythiophene derivatives, Chem. Mater. 9 (1997) 2902-2905.
[34] B. Ecker, J. C. Nolasco, J. Pallarés, L. F. Marsal, J. Posdorfer, J. Parisi, E. von Hauff, Degradation effects related to the hole transport layer in organic solar cells, Adv. Funct. Mater., 21 (2011) 2705-2711.
[35] Y. H. Zhou, C. Fuentes-Hernandez, J. Shim, J. Meyer, A. J. Giordano, H. Li, P. Winget, T. Papadopoulos, H. Cheun, J. Kim, M. Fenoll, A. Dindar, W. Haske, E. Najafabadi, T. M. Khan, H. Sojoudi, S. Barlow, S. Graham, J. L. Brédas, S. R. Marder, A. Kahn, B. Kippelen, A universal method to produce low–work function electrodes for organic electronics, Science 336 (2012) 327-332.
[36] C. H. Duan, W. Z. Cai, B. B. Y. Hsu, C. M. Zhong, K. Zhang, C. C. Liu, Z. C. Hu, F. Huang, G. C. Bazan, A. J. Heeger, Y. Cao, Toward green solvent processable photovoltaic materials for polymer solar cells: the role of highly polar pendant groups in charge carrier transport and photovoltaic behavior, Energy Environ. Sci., 6 (2013) 3022-3034.

[37] J. Kesters, T. Ghoos, H. Penxten, J. Drijkoningen, T. Vangerven, D. M. Lyons, B. Verreet, T. Aernouts, L. Lutsen, D. Vanderzande, J. Manca, W. Maes, Imidazolium-substituted polythiophenes as efficient electron transport materials improving photovoltaic performance, Adv. Energy Mater. 3 (2013) 1180-1185.